Brownian self-driven particles on the surface of a sphere

Leonardo Apaza[1] and Mario Sandoval[2,*]

[1]*Faculty of Pure and Natural Sciences, Universidad Mayor de San Andres, La Paz, Bolivia*

[2]*Department of Physics, Universidad Autonoma Metropolitana-Iztapalapa, Mexico City 09340, Mexico*

(Received 28 May 2017; revised manuscript received 3 July 2017; published 10 August 2017)

We present the dynamics of overdamped Brownian self-propelled particles moving on the surface of a sphere. The effect of self-propulsion on the diffusion of these particles is elucidated by determining their angular (azimuthal and polar) mean-square displacement. Short- and long-times analytical expressions for their angular mean-square displacement are offered. Finally, the particles' steady marginal angular probability density functions are also elucidated.

DOI: 10.1103/PhysRevE.96.022606

I. INTRODUCTION

Motion of particles on curved surfaces at microscopic level is a very common situation in nature. Some relevant examples are the motion of proteins on the surface of eukaryotic cells [1], the reaction of T cells from the immunological system to antigens located on artificial curved surfaces [2], or self-driven microtubule bundles moving on the surface of droplets [3]. At these scales, Brownian motion may play an important role on the dynamics of such a small systems. In this sense, there have been several works modeling the motion of micrometric particles on simple curved surfaces like the sphere. For example, Brillinger studied the diffusion of particles with constant drift able to move on the surface of a sphere [4]. Krishna *et al.* [5] analytically found the solid angle distribution enclosed by Brownian particles displacing on a sphere. Batada *et al.* [1] found an analytical expression for the rate at which proteins on a cell surface membrane (modeled as a sphere) meet. Using matched asymptotic expansions Coombs *et al.* [2] found analytical expressions for the rate at which particles on a sphere are captured by localized traps. New algorithms to generate Brownian motion on a sphere have been also reported [6,7]. Additionally, a theoretical propagator for diffusion on a sphere equivalent to the Gaussian propagator of diffusion on flat surfaces was proposed by Ghosh *et al.* [8].

Note that most of the previous works have treated passive (non-self-propelled) particles. Recently, the inclusion of an internal energy to Brownian particles that allow them to self-propel, has shown to be a broader model to study many out of equilibrium natural and artificial scenarios, such as the organization of motile cells or the motion of natural (swimming microorganisms) and synthetic (microrobots) microparticles [9–12]. Related works dealing with self-propelled particles moving on curved surfaces are Sanchez *et al.* [3]. They studied self-driven microtubule bundles on the surface of a droplet and observed the emergence of a streaming flow. Großmann *et al.* [13] assumed that the director vector (swimming direction vector) of active Brownian particles (ABPs) does not necessarily move on a sphere, thus they study the case of a director vector moving for example on an ellipsoid. They find that if the director vector of ABPs moves on a hypersphere their diffusion will be isotropic, whereas their diffusion becomes anisotropic if the director moves on a deformed hypersphere. More recently, Sknepnek and Henkes [3] studied collective behavior of active particles constrained to move on a sphere. They found that curvature induces, among other patterns, polar vortex and circulating bands states similar to what experimentalists found [14]. In addition, Janssen *et al.* [15] studied the motion of self-propelled particles (spheres and rods) on a sphere, and for various particles' densities. They confirmed that topological constrains give rise to novel patterns that cannot be seen on flat surfaces. A theoretical study on the dynamics of active particles performing rotational Brownian motion on curved surfaces has also been recently presented by Fily *et al.* [16].

Motivated by the previous works, in this paper we extend the well-known motion of Brownian passive particles on a sphere, to the out of equilibrium situation of active (self-propelling) Brownian particles displacing on a sphere. Following a Langevin approach, it is possible to analytically obtain, for both passive and active particles, their angular mean-square displacement (MSD) at short ($t \to 0$) and long ($t \to \infty$) times. Our theoretical results were compared with Brownian dynamics simulations and an excellent agreement was found. At short times a linear dependence in time for both azimuthal and polar MSDs was obtained. For long times, and for both passive and active particles, their steady state angular probability density functions (PDFs) were numerically reached. Analytical expressions are also offered. A comparison between passive and active results is also made, and we find that the steady polar marginal PDF of passive and active particles are the same.

II. MODEL

Let us analyze Brownian self-propelled particles (swimmers) of radius a moving on the surface of a sphere of radius r. Based on a spherical coordinates' system (ϕ,θ), it is possible to identify the unit vectors $(\widehat{e}_\phi,\widehat{e}_\theta)$ which form a tangential plane on the sphere's surface (see Fig. 1). Using this instantaneous tangential plane, we introduce the swimming velocity term $\mathbf{U} = U\widehat{\mathbf{u}}(t)$, being $\widehat{\mathbf{u}}(t) = v_\phi(t)\widehat{e}_\phi + v_\theta(t)\widehat{e}_\theta$, the instantaneous unit vector in the direction of swimming. Here U is the magnitude of the swimming velocity which is taken to be constant for simplicity. Thermal fluctuations in translation, $\mathbf{f}(t) = f_\phi(t)\widehat{e}_\phi + f_\theta(t)\widehat{e}_\theta$, and rotation, $\mathbf{g}(t) = \sqrt{2D_R}\eta_\theta\hat{e}_\theta + \sqrt{2D_R}\eta_\phi\hat{e}_\phi$, (where η_θ and η_ϕ are independent white noise

*sem@xanum.uam.mx

 ©2017 American Physical Society

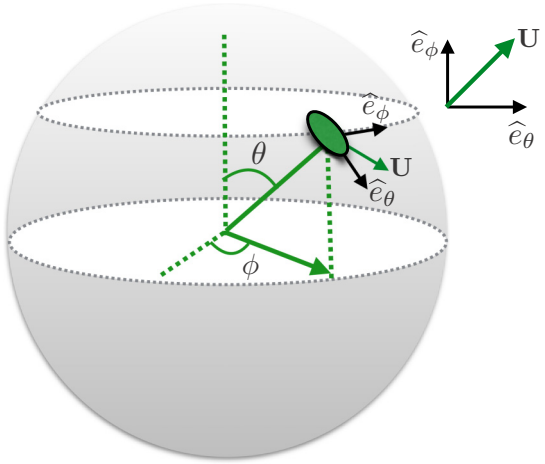

FIG. 1. Schematics of the studied problem.

processes, while D_R is a rotational diffusivity constant) are also included, hence the equations of motion for a swimmer can be written as

$$m(\ddot{\theta} - \cos\theta \sin\theta \dot{\phi}^2) = -\gamma_T \dot{\theta} + \gamma_T U \frac{v_\theta}{r} + f_\theta, \quad (1)$$

$$m(\ddot{\phi} + 2\cot\theta \dot{\theta}\dot{\phi}) = -\gamma_T \dot{\phi} + \gamma_T U \frac{v_\phi}{r \sin\theta} + f_\phi, \quad (2)$$

$$\dot{v}_\theta = \sqrt{2D_R} v_\phi (\eta_\theta v_\phi - \eta_\phi v_\theta) + \cos\theta v_\phi \dot{\phi}, \quad (3)$$

$$\dot{v}_\phi = \sqrt{2D_R} v_\theta (\eta_\phi v_\theta - \eta_\theta v_\phi) - \cos\theta v_\theta \dot{\phi}, \quad (4)$$

where m is the mass of the swimmer, while γ_T and γ_R are the resistance coefficients to translation and rotation respectively. Equations (3) and (4) are obtained by projecting the dynamics of the orientation vector onto the contravariant local basis (e^ϕ, e^θ) [16]. At this stage we recall the Smoluchowsky diffusion equation for the probability density function, P, of an overdamped passive Brownian particle on the surface of a sphere, namely,

$$\frac{\partial P}{\partial t} = \frac{D_T}{r^2 \sin\theta} \frac{\partial}{\partial \theta}\left(\sin\theta \frac{\partial P}{\partial \theta} \right) + \frac{D_T}{r^2 \sin^2\theta} \frac{\partial^2 P}{\partial \phi^2}. \quad (5)$$

where D_T is a translational diffusivity constant. With Eq. (5), one can formulate its respective Langevin equations [4], namely, $\dot{\phi} = (\sqrt{2D_T}/r \sin\theta)\xi_\phi$ and $\dot{\theta} = D_T/r^2 \tan\theta + (\sqrt{2D_T}/r)\xi_\theta$, where the stochastic variables ξ_θ and ξ_ϕ, are independent white noise processes (zero mean and δ-correlated). Neglecting inertia (overdamped limit) in Eqs. (1) and (2) and using the previous Langevin equations that generate Eq. (5), we can explicitly write our Langevin model for active Brownian particles on the surface of a sphere, namely,

$$\dot{\theta} = \frac{U v_\theta}{r} + \frac{D_T}{r^2 \tan\theta} + \frac{\sqrt{2D_T}}{r} \xi_\theta, \quad (6)$$

$$\dot{\phi} = \frac{U v_\phi}{r \sin\theta} + \frac{\sqrt{2D_T}}{r \sin\theta} \xi_\phi, \quad (7)$$

$$\dot{v}_\theta = \sqrt{2D_R} v_\phi (\eta_\theta v_\phi - \eta_\phi v_\theta) + \cos\theta v_\phi \dot{\phi}, \quad (8)$$

$$\dot{v}_\phi = \sqrt{2D_R} v_\theta (\eta_\phi v_\theta - \eta_\theta v_\phi) - \cos\theta v_\theta \dot{\phi}. \quad (9)$$

Note that for the passive case, the polar coordinate Eq. (6) is decoupled from the azimuthal coordinate; however, the azimuthal coordinate is coupled to both the swimming direction and the polar coordinate. This coupling will be appreciated when solving the mean-square angular displacements at short times. In this situation, the term $\langle(\phi - \phi_0)^2\rangle$ will depend on θ_0 as it will be shown in the following section.

III. BROWNIAN MOTION ON A SPHERE: PASSIVE CASE

Let us approximately solve the stochastic Langevin Eqs. (6) and (7) for $U = 0$ (passive case). To do so, lets consider that our particle is initially located at around $\theta_0 = \pi/2$; hence, at very short times, one can find that $\theta(t) - \theta_0 \simeq \int_0^t (\sqrt{2D_T}/r)\xi_\theta(t')dt'$, from which we easily get

$$\langle(\theta - \theta_0)^2\rangle \simeq \frac{2D_T}{r^2} t. \quad (10)$$

The latter result was observed to be very robust and remains valid for even $0 < \theta_0 < \pi$. The inset of Fig. 2(b) shows this observation, where different initial conditions for the polar variable namely, $\theta_0 = \{0.02, 0.2, 0.4, 0.6\}$, are considered.

In the case of Eq. (7), we use that Eq. (10) is still valid for $\theta_0 \ll 1$, which implies that for very short times, $\theta \ll 1$; hence, $1/\sin(\theta) \simeq 1/\theta + \theta/6$. Thus, we get from Eq. (7) that $\phi(t) - \phi_0 \simeq (\sqrt{2D_T}/r) \int_0^t [\theta^{-1}(t') + \theta(t')/6]\xi_\phi(t')dt'$. Using the latter expression to perform the product $[\phi(t) - \phi_0]^2$, noticing that $[1 + (\sqrt{2D_T}/r) \int_0^t \xi_\theta(t')dt']^{-1} \simeq 1 - (\sqrt{2D_T}/r) \int_0^t \xi_\theta(t')dt'$, and performing an ensemble average we get

$$\langle(\phi(t) - \phi_0)^2\rangle \simeq \frac{2D_T}{\theta_0^2 r^2} t. \quad (11)$$

The above result provides a good estimate for the range $0 < \theta_0 < \pi/2$, and by symmetry we can also approximate the azimuthal MSD for $\pi/2 < \theta_0 < \pi$ as $\langle(\phi(t) - \phi_0)^2\rangle \simeq 2D_T(\theta_0 - \pi)^{-2}/r^2$. The latter approximations are less accurate for θ_0 around $\pi/2$. However, one can construct a better expression for the case θ_0 around $\pi/2$ by adding the previous results, which is $\langle(\phi(t) - \phi_0)^2\rangle \simeq 2D_T(\theta_0^{-2} + (\theta_0 - \pi)^{-2})/r^2$. Notice from Eq. (11) the dependence of the azimuthal MSD on the polar initial condition. This dependence is numerically corroborated in Fig. 2(a).

We now turn to characterize the passive Brownian motion at long times. To do so, we recall that Eq. (5) has the solution [17],

$$P(\theta,\phi;t) = \sum_{k=0}^{\infty} \sum_{m=-k}^{k} e^{-k(k+1)D_T t/r^2} Y_k^m(\theta,\phi) Y_k^m(\theta_0,\phi_0), \quad (12)$$

where $Y_k^m(\theta,\phi)$ are the spherical harmonics. Given Eq. (12), the steady marginal probability density functions can be found as

$$p(\theta) = \lim_{t\to\infty} \int_0^{2\pi} P(\theta,\phi;t)\sin(\theta)d\phi = \frac{\sin(\theta)}{2}, \quad (13)$$

$$p(\phi) = \lim_{t\to\infty} \int_0^{\pi} P(\theta,\phi;t)\sin(\theta)d\theta = \frac{1}{2\pi}. \quad (14)$$

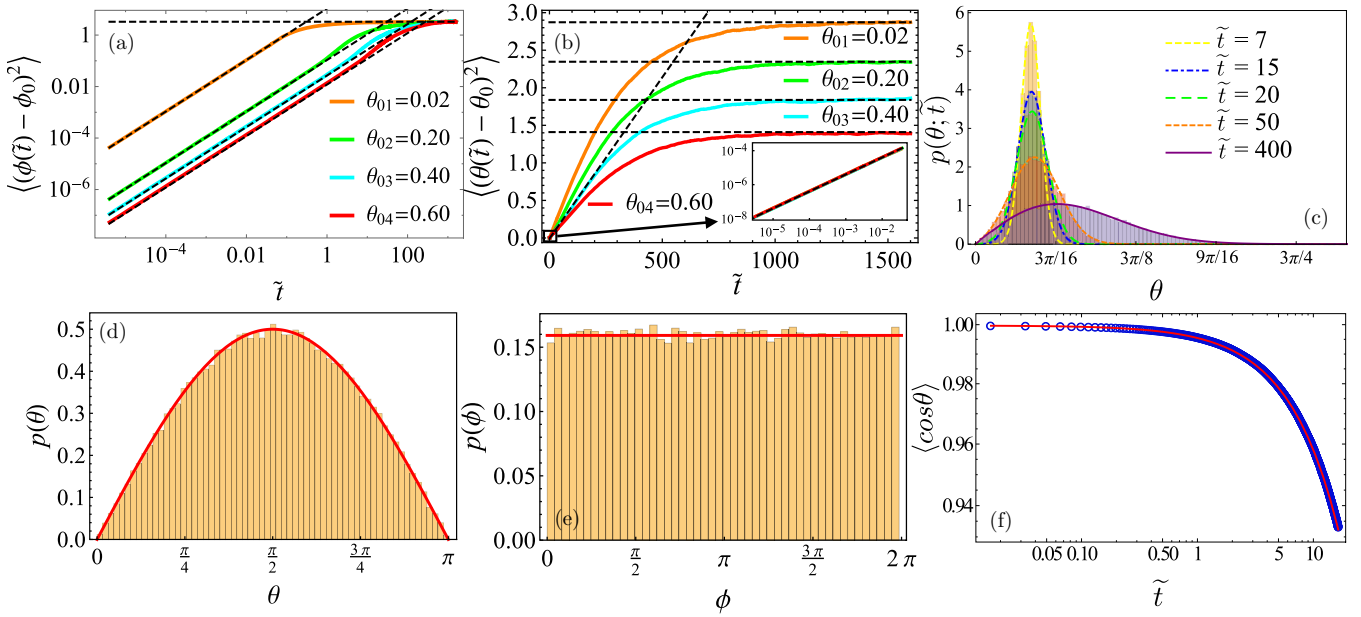

FIG. 2. Comparison between theory and Brownian dynamics simulations for passive particles diffusing on a sphere. (a, b) Angular mean-square displacements versus time. The theoretical short times [Eqs. (10) and (11)] and long times [Eqs. (16) and (17)] results for different initial conditions are presented in dashed lines, while the numerical results are in solid lines. (c) Time evolution of the marginal polar PDF. The analytical results for $p(\theta;t)$ are presented in dashed and solid lines, whereas the numerical results are represented with bars. (d, e) Marginal steady PDFs. The theoretical expressions given by Eq. (13) and (14) are presented in solid (red) lines, while the numerical results appear with bars. (f) The theoretical value $\langle\cos\theta\rangle = \exp(-2D_T t/r^2)$ (solid red line) is compared with its numerical value (blue circles).

Using the previous marginal PDFs and the definition of ensemble average,

$$\langle f(\theta,\phi)\rangle = \int_0^{\pi} d\theta \int_0^{2\pi} d\phi\, f(\theta,\phi) \lim_{t\to\infty} P(\theta,\phi;t)\sin(\theta), \tag{15}$$

together with $f(\theta,\phi) = (\theta-\theta_0)^2$ and $f(\theta,\phi) = (\phi-\phi_0)^2$, we get the long-term angular mean-square displacements,

$$\langle(\theta-\theta_0)^2\rangle = \frac{\pi^2-4}{2} + \theta_0(\theta_0-\pi), \tag{16}$$

$$\langle(\phi-\phi_0)^2\rangle = \frac{4\pi^2}{3} + \phi_0(\phi_0-2\pi). \tag{17}$$

The previous theoretical expressions were compared to Brownian dynamics simulations, and the results are presented in Fig. 2. Figures 2(a) and 2(b) show the angular mean-square displacements versus time. Here, the theoretical short times [Eqs. (10) and (11)] and long times [Eqs. (16) and (17)] results, are presented in dashed lines, while the numerical results are in solid lines. To see the dependence of the azimuthal mean-square displacement on the initial polar condition, Fig. 2(a) shows the results of four different values for this quantity, namely, $\theta_0 = \{0.02, 0.2, 0.4, 0.6\}$, while ϕ_0 was fixed to π. Note that $\tilde{t} = D_R t$. An excellent agreement between theory and numerics can be observed. Figure 2(b) shows the polar MSD for different initial conditions ($\theta_0 = \{0.02, 0.2, 0.4, 0.6\}$); here, the long-time result given by Eq. (16) is numerically corroborated. Figure 2(c) shows the time evolution of the marginal polar PDF, $p(\theta;t) = \int_0^{2\pi} P(\theta,\phi;t)\sin(\theta)d\phi$. The analytical results for $p(\theta;t)$ are presented in dashed and solid lines, whereas the numerical results are represented with bars. An excellent agreement is observed. The analytical expressions for the marginal steady PDFs [Eqs. (13) and (14)] are also numerically tested. This can be seen in Figs. 2(d) and 2(e), where the theoretical expressions given by Eqs. (13) and (14) (solid lines) are compared with the statistics (bars) generated from the Langevin Eqs. (6)–(8) for the case $U = 0$. An excellent agreement between numerics and theory is observed. Finally, the mean of the cosine of the angular coordinate $\langle\cos\theta\rangle$, whose theoretical value is $\langle\cos\theta\rangle = \exp(-2D_T t/r^2)$, is also plotted in Fig. 2(f). The theoretical value is represented in solid (red) line while the numerical value taken from Eqs. (6)–(8) for the case $U = 0$, is plotted in (blue) circles. Note that Fig. 2 can also be regarded as a validation of the Langevin model we are implementing. In the following section we extend our results to the case of active (self-propelled) Brownian particles.

IV. BROWNIAN MOTION ON A SPHERE: ACTIVE CASE

We now use Brownian dynamics simulations to solve the stochastic Langevin Eqs. (6)–(9) for the case of active Brownian particles moving on the surface of a sphere of radius r. Let us introduce the dimensionless time $\tilde{t} = D_R t$, the dimensionless numbers $Pe_R = U D_R^{-1}/r$ (which is the ratio between the persistence length of swimmers and the radius of the sphere), and $\bar{\kappa} = D_T/r^2 D_R = (4/3)(a/r)^2$. Note that the curvature of the system is $\kappa = 1/r$; hence, $\bar{\kappa}$ represents the product of the swimmer's radius with the sphere's curvature. With the latter dimensionless quantities system Eqs. (6)–(9)

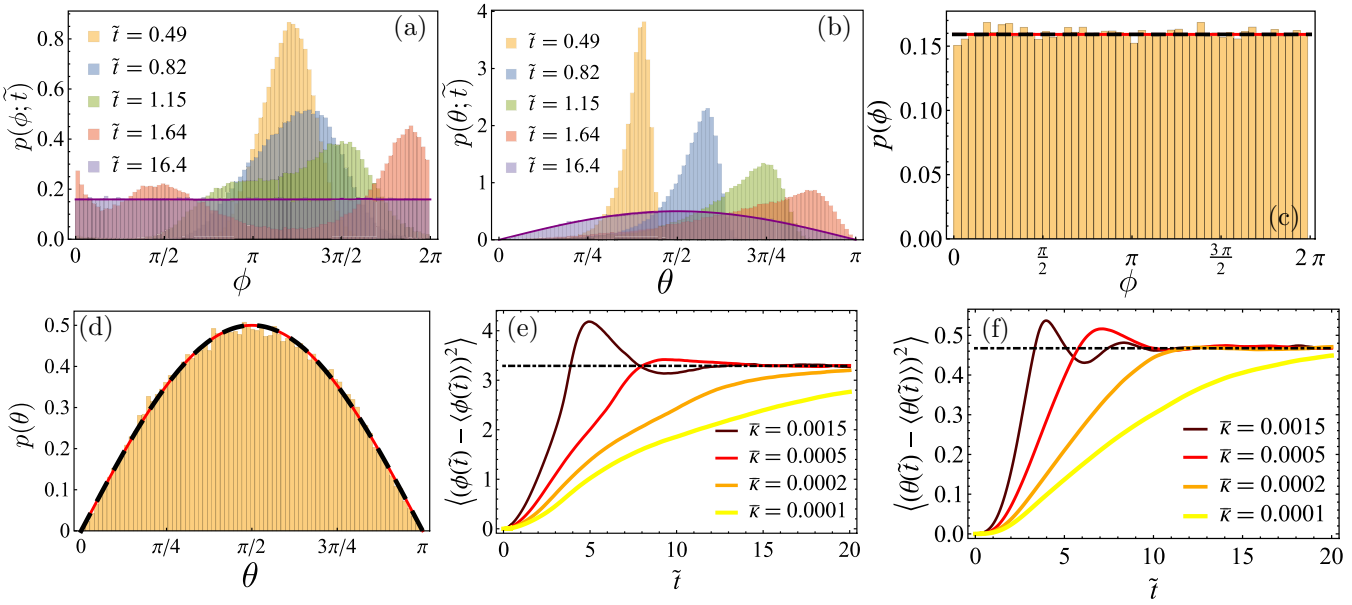

FIG. 3. Comparison between theory and Brownian dynamics simulations for active particles diffusing on a sphere. (a, b) Time evolution of the marginal angular PDFs for $(Pe_R,\bar{\kappa})$ set to (1.95,0.0021). Here, Eqs. (22) and (23) were numerically solved using the statistics generated from Eqs. (18)–(21). (c, d) Steady marginal angular PDFs. From these figures one infers that for ABPs $p(\theta) = \sin(\theta)/2$ and $p(\phi) = 1/2\pi$ (black dashed lines). In the same figures, we superpose in red solid lines, the steady marginal PDFs for the passive case. Note that for the polar and azimuthal angles, passive and active marginal steady PDFs coincide. (e, f) Curvature effect on the angular MSD. Here, the dimensionless number $\bar{\kappa}$ was taken as $\bar{\kappa} = \{0.0001,0.0002,0.0005,0.0015\}$. The theoretical results given by Eqs. (24) and (25) are presented in dotted-dashed black lines.

becomes

$$\dot{\theta} = Pe_R v_\theta + \frac{\bar{\kappa}}{\tan\theta} + \sqrt{2\bar{\kappa}}\xi_\theta, \tag{18}$$

$$\dot{\phi} = \frac{Pe_R v_\phi}{\sin\theta} + \frac{\sqrt{2\bar{\kappa}}}{\sin\theta}\xi_\phi, \tag{19}$$

$$\dot{v}_\theta = \sqrt{2}v_\phi(\eta_\theta v_\phi - \eta_\phi v_\theta) + \cos(\theta)v_\phi\dot{\phi}, \tag{20}$$

$$\dot{v}_\phi = \sqrt{2}v_\theta(\eta_\phi v_\theta - \eta_\theta v_\phi) - \cos(\theta)v_\theta\dot{\phi}. \tag{21}$$

To numerically solve the previous system, a step size of $\Delta\tilde{t} = 0.001$ and 30 000 realizations were considered. We randomly choose the initial conditions $(\theta_0,\phi_0,v_\phi(0),v_\theta(0)) = (0.4,\pi,1/\sqrt{2},1/\sqrt{2})$. Figures 3(a) and 3(b) show the time evolution (five different times) of the marginal angular PDFs defined as

$$p(\theta;t) = \int_{-1}^{1}\int_{-1}^{1}\int_{0}^{2\pi} P(\theta,\phi,v_\theta,v_\phi;t)\sin\theta dv_\theta dv_\phi d\phi, \tag{22}$$

$$p(\phi;t) = \int_{-1}^{1}\int_{-1}^{1}\int_{0}^{\pi} P(\theta,\phi,v_\theta,v_\phi;t)\sin\theta dv_\theta dv_\phi d\theta. \tag{23}$$

Here, the parameters $(Pe_R,\bar{\kappa})$ were set to (1.95,0.0021). Note that Eqs. (22) and (23) are numerically solved using the statistics generated from Eqs. (18)–(21). For longer times, one can observe that the marginal PDFs reach a steady state. This is shown in Figs. 3(c) and 3(d). From this figure, one infers that the steady marginal angular PDFs for ABPs are $p(\theta) = \sin\theta/2$ and $p(\phi) = 1/2\pi$ [black dashed lines in Figs. 3(c) and 3(d)]. In the same two figures, we superpose in red solid lines, the steady marginal PDFs for passive particles. One observes that for the azimuthal and polar angles, both passive and active marginal steady PDFs coincide. This result reflects the symmetry property (rotational invariance) of a sphere.

We now turn to calculate the long time angular MSD. To do so, we use Eq. (15) together with the respective active steady PDFs to perform the integral. Note that for the Brownian motion on a sphere, the mean of the angular variables will not always coincide with their initial values (θ_0,ϕ_0). For example, at short times, we have that $\lim_{\tilde{t}\to 0}\langle\theta(\tilde{t})\rangle = \theta_0$ and $\lim_{\tilde{t}\to 0}\langle\phi(\tilde{t})\rangle = \phi(0) = \phi_0$, whereas at long times one can show that $\lim_{\tilde{t}\to\infty}\langle\theta(\tilde{t})\rangle = \pi/2$ and $\lim_{\tilde{t}\to\infty}\langle\phi(\tilde{t})\rangle = \pi$. Thus, one should rigorously define the MSD as the mean-square deviation from the mean (formally the variance for this case). Using this fact, we arrive to the following long-times results:

$$\langle(\theta(\tilde{t}) - \langle\theta(\tilde{t})\rangle)^2\rangle = \frac{\pi^2 - 8}{4}, \tag{24}$$

$$\langle(\phi(\tilde{t}) - \langle\phi(\tilde{t})\rangle)^2\rangle = \frac{\pi^2}{3}, \tag{25}$$

which are also valid for passive particles. The curvature effect on the angular MSD is shown in Figs. 3(e) and 3(f). Here the dimensionless number $\bar{\kappa}$ was taken as $\bar{\kappa} = \{0.0001, 0.0002, 0.0005, 0.0015\}$. These figures simply show that as the radius of the sphere decreases ($\bar{\kappa}$ increasing), the particles will reach is steady state faster. In other words, particles sample the entire sphere's surface faster as the sphere's radius decreases.

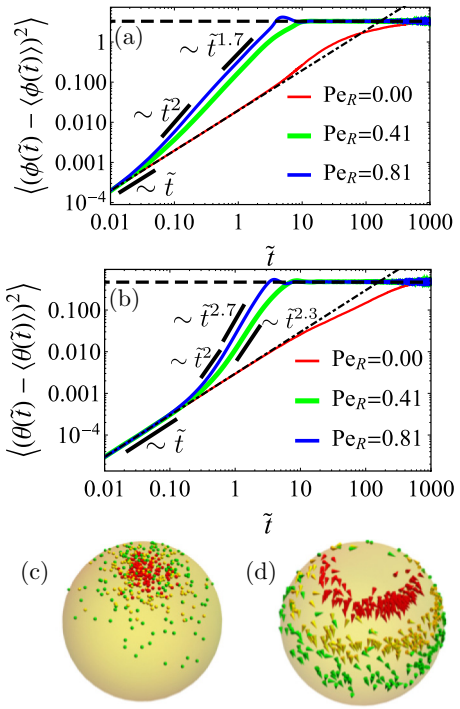

FIG. 4. (a, b) Comparison between theoretical results and Brownian dynamics simulations for different swimming velocities namely, $Pe_R = \{0,0.41,0.81\}$, and for the same curvature parameter $\overline{\kappa} = 0.0015$. Here, the dashed lines represent the theoretical long time MSD results given by Eqs. (24) and (25). The short times results [Eqs. (10) and (17)] are represented in dotted-dashed lines. Note that for comparison purposes, we have included in solid red lines, the results for passive particles. (c) Passive Brownian particles ($Pe_R = 0$) on a sphere with $\overline{\kappa} = 0.0015$ and for $\tilde{t} = \{5\,(\text{red}), 25\,(\text{yellow}), 50\,(\text{green})\}$. (d) Active Brownian particles ($Pe_R = 0.81$) with $\overline{\kappa} = 0.0015$ and for $\tilde{t} = \{0.74\,(\text{red}), 1.29\,(\text{yellow}), 1.79\,(\text{green})\}$. In both cases, $\theta_0 = 0.4$ and $\phi_0 = \pi$.

Let us finally verify Eqs. (24) and (25). To do so, we perform Brownian dynamics simulations for different swimming velocities namely, $Pe_R = \{0,0.41,0.81\}$, and for the same curvature parameter $\overline{\kappa} = 0.0015$. The results are shown in the Log-Log Figs. 4(a) and 4(b), where the dashed lines represent the theoretical long time results given by Eqs. (24) and (25), whereas the short times results [Eqs. (10) and (11)] are represented by black dashed-dotted lines. The numerical results are shown in solid lines. Figures 4(a) and 4(b) show that for short times, Eqs. (10) and (11) are still valid for active particles, and that similar to ABPs on a flat surface [18], the angular MSD of ABPs on curved surfaces has also a linear (short times) and quadratic dependence (due to self-propulsion) on time. Note that the angular MSD starts linearly in time since we are considering the overdamped regime. Intermediate super-diffusive regions are also observed which is similar to the behavior of ABPs on flat surfaces *et al.* [18].

Figures 4(a) and 4(b) also indicate that the long time angular MSD, for both passive (red solid line) and active cases, coincides. One can also see that self-propulsion enables the system to reach its steady state in a shorter period of time compared to passive particles. Finally, Figs. 4(c) and 4(d) visually indicates the effect of self-propulsion on the diffusion of Brownian particles. Figure 4(c) represents passive Brownian particles ($Pe_R = 0$) on a sphere with $\overline{\kappa} = 0.0015$ and for $\tilde{t} = \{5\,(\text{red}), 25\,(\text{yellow}), 50\,(\text{green})\}$, while Fig. 4(d) shows active Brownian particles ($Pe_R = 0.81$) with $\overline{\kappa} = 0.0015$ and for $\tilde{t} = \{0.74\,(\text{red}), 1.29\,(\text{yellow}), 1.79\,(\text{green})\}$. In both cases, $\theta_0 = 0.4$ and $\phi_0 = \pi$. Clearly, self-propulsion enables the particle to sample the entire sphere's surface in a shorter amount of time.

V. CONCLUSIONS

In summary, we have studied the effect of self-propulsion and curvature on the diffusion of active Brownian particles (ABPs) on the surface of a sphere. Basically, as self-propulsion increases, the particles reach their steady state in a shorter amount of time compared to passive particles. In the same way, as the radius of the sphere decreases ($\overline{\kappa}$ increasing), the particles will reach is steady state in a shorter time since the area to sample is smaller. To quantify the latter observations, analytical expressions for the the steady angular marginal PDFs, and for the angular mean-square displacements (short and long times) for both passive and active Brownian particles were found. We found that the steady angular (azimuthal and polar) marginal PDFs of passive and active particles are the same, thus recovering the rotational invariance of a sphere. Brownian dynamics simulations were also performed and an excellent agreement between theory and simulations for both passive and active particles was observed.

ACKNOWLEDGMENTS

M.S. and L.A. thank Consejo Nacional de Ciencia y Tecnologia, for support through CONACyT Grant No. CB 2014/237848. The authors sincerely thank an anonymous referee for his very relevant comments.

[1] N. Batada, L. Shepp, D. Siegmund, and M. Levitt, PLoS Comput. Biol. **2**, e34 (2006).
[2] D. Coombs, R. Straube, and M. Ward, SIAM J. Appl. Math. **70**, 302 (2009).
[3] T. Sanchez, D. T. Chen, S. J. DeCamp, M. Heymann, and Z. Dogic, Nature **491**, 431 (2012).
[4] D. R. Brillinger, J. Theor. Prob. **10**, 429 (1997).
[5] M. M. G. Krishna, J. Samuel, and S. Sinha, J. Phys. A: Math. Gen. **33**, 5965 (2000).
[6] T. Carlsson, T. Ekholm, and C. Elvingson, J. Phys. A: Math. Theor. **43**, 505001 (2010).
[7] P. Castro-Villarreal, A. Villada-Balbuena, J. M. Mendez-Alcaraz, R. Castaneda-Priego, and S. Estrada-Jimenez, J. Chem. Phys. **140**, 214115 (2014).

[8] A. Ghosh, J. Samuel, and S. Sinha, Europhys. Lett. **98**, 30003 (2012).
[9] M. C. Marchetti, J. F. Joanny, S. Ramaswamy, T. B. Liverpool, J. Prost, M. Rao, and R. A. Simha, Rev. Mod. Phys. **85**, 1143 (2013).
[10] C. Bechinger, R. D. Leonardo, H. Löwen, C. Reichhardt, G. Volpe, and G. Volpe, Rev. Mod. Phys. **88**, 045006 (2016).
[11] M. F. Hagan and A. Baskaran, Curr. Opin. Cell Biol. **38**, 74 (2016).
[12] S. Ebbens, Curr. Opin. Colloid Interface Sci. **21**, 14 (2016).
[13] R. Großmann, F. Peruani, and M. Bär, Eur. Phys. J. Special Topics **224**, 1377 (2015).
[14] R. Sknepnek and S. Henkes, Phys. Rev. E **91**, 022306 (2015).
[15] L. M. C. Janssen, A. Kaiser, and H. Löwen, Sci. Rep. **7**, 5667 (2017).
[16] Y. Fily, A. Baskaran, and M. F. Hagan, arXiv:1601.00324.
[17] K. Yosida, Annu. Math. Stat. **20**, 292 (1949).
[18] B. ten Hagen, S. van Teeffelen, and H. Lowen, J. Phys.: Condens. Matter **23**, 194119 (2011).